Journal of ELECTRONIC MATERIALS, Vol. 46, No. 1, 2017
DOI: 10.1007/s11664-016-4894-6

Highly Visible Light Activity of Nitrogen Doped TiO_2 Prepared by Sol–Gel Approach

LE DIEN THAN,[1] NGO SY LUONG,[2] VU DINH NGO,[1] NGUYEN MANH TIEN,[1] TA NGOC DUNG,[3] NGUYEN MANH NGHIA,[4] NGUYEN THAI LOC,[5] VU THI THU,[6] and TRAN DAI LAM[7,8,9,10]

1.—Viet Tri University of Industry, 9 Tien Son street, Phu Tho, Viet Tri, Viet Nam. 2.—Hanoi University of Science, 19 Le Thanh Tong Road, Ha Noi, Viet Nam. 3.—Ha Noi University of Science and Technology, 1 Dai Co Viet, Ha Noi, Viet Nam. 4.—Hanoi National University of Education, 136 Xuan Thuy, Ha Noi, Viet Nam. 5.—Asian Institute of Technology, Klong Luang, PO Box 4, Pathumthani, Bangkok 12120, Thailand. 6.—Hanoi University of Science and Technology, Vietnam Academy of Science and Technology, 18 Hoang Quoc Viet Road, Ha Noi, Viet Nam. 7.—Graduate University of Science and Technology, Vietnam Academy of Science and Technology, 18 Hoang Quoc Viet Road, Ha Noi, Viet Nam. 8.—Duy Tan University, 182 Nguyen Van Linh Road, Da Nang, Viet Nam. 9.—e-mail: trandailam@gmail.com. 10.—e-mail:tdlam@gust-edu.vast.vn

A simple approach was explored to prepare N-doped anatase TiO_2 nanoparticles (N-TiO_2 NPs) from titanium chloride ($TiCl_4$) and ammonia (NH_3) via sol–gel method. The effects of important process parameters such as calcination temperatures, $NH_3/TiCl_4$ molar ratio (R_N) on crystallite size, structure, phase transformation, and photocatalytic activity of titanium dioxide (TiO_2) were thoroughly investigated. The as-prepared samples were characterized by ultraviolet–visible spectroscopy, x-ray diffraction, transmission electron microscopy, energy dispersive x-ray spectroscopy, and x-ray photoelectron spectroscopy. The photocatalytic activity of the samples was evaluated upon the degradation of methylene blue aqueous solution under visible-light irradiation. The results demonstrated that both calcination temperatures and $NH_3/TiCl_4$ molar ratios had significant impacts on the formation of crystallite nanostructures, physicochemical, as well as catalytic properties of the obtained TiO_2. Under the studied conditions, calcination temperature of 600°C and $NH_3/TiCl_4$ molar ratio of 4.2 produced N-TiO_2 with the best crystallinity and photocatalytic activity. The high visible light activity of the N-TiO_2 nanomaterials was ascribed to the interstitial nitrogen atoms within TiO_2 lattice units. These findings could provide a practical pathway capable of large-scale production of a visible light-active N-TiO_2 photocatalyst.

Key words: TiO_2, anatase, visible-light activity, photocatalyst, interstitial nitrogen, sol–gel

INTRODUCTION

In recent years, photocatalytic detoxification of water and air has attracted considerable attention.[1,2] Among several photocatalysts being investigated, titanium dioxide is highly preferred due to its low-cost of production, strong catalytic activity, stability, and nontoxicity.[3,4] However, the large band gap (3.2 eV) of TiO_2 restricts its applications mainly to the ultraviolet (UV) ranges, which account for only 3–5% of sunlight energy.[3] Photocatalytic efficiency of TiO_2 could be enhanced by generating mid-gap states or narrow its band gap.[5] The most effective method is to dope TiO_2 with impurities such as metal [iron (Fe) and copper (Cu)] or non-metal elements [boron (B), carbon (C), nitrogen (N), sulfur (S), and fluorine (F)].[6–10] However,

(Received January 21, 2016; accepted August 19, 2016; published online September 6, 2016)

metal doping can lead to thermal instability and carrier trapping which may adversely affect the photocatalytic power of the obtained catalysts.[9] Regarding the widely used non-metal dopants, nitrogen (N) reportedly exhibits considerable absorption in the visible wavelengths.[9–11] Moreover, nitrogen is greatly desirable due to its nontoxic nature and proven ability to enhance photocatalytic efficiency of TiO_2.[2] So far, the effects of N doping on photocatalytic enhancement of TiO_2 have not been fully understood even though several mechanisms such as the mixing the N 2*p* with O 2*p* states, the formation of N-induced midgap levels or impurity species such as NO_x, NH_x have been proposed.[12] Recent studies have also reported that oxygen vacancy or associated defects within TiO_2 plays a vital role in the visible-light activity (VLA) of N-TiO_2.[13–15]

The synthesis of N-doped TiO_2 can be conducted by various methods such as sputtering,[16,17] ion implantation,[18] chemical vapor deposition,[19,20] sol–gel,[21–25] oxidation of TiN,[26] nitrification of TiO_2 in an ammonia gas flow,[9] or decomposition of N-containing metal organic precursors.[27] However, large-scale applications of N-TiO_2 are feasible only if this material can be produced by simple, inexpensive technologies and equipment. The sol–gel method could be a viable choice as N-doped TiO2 can be simply produced by adding a nitrogen precursor (NH_4Cl or NH_4OH) a solution containing Titanium anions. In one study by Sato et al.[24] N-TiO_2 with evident VLA was obtained, simply by annealing the mixture of $Ti(OH)_4$ and either NH_4Cl or NH_4OH.

The photocatalytic activity of N-TiO_2 can be significantly affected by the structure and sizes of TiO_2 crystallites, level and chemical states of doped nitrogen.[28–30] For example, it was believed that the N-TiO_2 crystals in anatase phase showed better photocatalytic activity, compared to N-TiO_2 crystals in other phases.[2] The effect of nitrogen level on structural properties and photocatalytic activity of N-TiO_2 were reported by many authors.[25,27,29,30] Sato et al.[25] has demonstrated that the photocatalytic activity of N-TiO_2 increased with increasing calcination temperature up to around 400°C and then decreased with further increase in calcination temperatures. The authors ascribed the increase and decrease in catalytic activity to narrowed bandgap of doped samples and the sintering of the samples, respectively. Therefore, it is critical to control the physical behaviors of N-TiO_2 crystals in order to maximize its photocatalytic activity.

In this study, a simple approach for preparing N-TiO_2 from calcined products of $TiCl_4$ in NH_4OH was reported. This sol–gel method enabled massive production of highly active photocatalyst for applications in water treatments. The effects of calcination temperatures and molar ratio of $NH_3/TiCl_4$ on crystallite structure, chemical states of doped N, VLA of N-TiO_2 were thoroughly investigated.

MATERIALS AND METHODS

Materials

Titanium chloride ($TiCl_4$, 99%) was purchased from Sigma-Aldrich and used without further purification. Ammonia (NH_3, 25%) and methylene blue (MB) were purchased from Merck. Other chemicals were of analytical grades.

Preparation of N-TiO_2 Nanoparticles

N-TiO_2 was synthesized by sol–gel method, using titanium chloride ($TiCl_4$) and ammonia (NH_3) as titanium source and dopant, respectively. Initially, 0.35 M $TiCl_4$ solution (solution A) was prepared via the hydrolysis of titanium chloride (99%) in water at 0°C. Aqueous ammonia (10%) (solution B) was prepared at 0°C from stock solution (25%) and was then mixed with solution A at given $NH_3/TiCl_4$ molar ratios (R_N = 0–4.2). The mixture was vigorously stirred at ambient temperature for 4 h. The precipitate was filtered, washed four times by distilled water before being dried at 60°C for 24 h in a vacuum drying cabinet.

To study the influence of calcination temperatures on phase transition, crystallite structure and photocatalytic activity of N-TiO_2, precursor mixtures of NH_3 and $TiCl_4$ (R_N = 4.2) were calcined at temperatures ranging from 200 to 900°C (heating rate 5°C/min) for 30 min. On the other hand, the effects of various $NH_3/TiCl_4$ molar ratios (0–4.2) on N-TiO_2 samples annealed at 600°C for 30 min were determined.

Characterization of N-Doped TiO_2

X-ray Diffraction (XRD)

X-ray diffraction (XRD) patterns of the as-prepared samples were recorded by powder x-ray diffractometer (D8 Advance Brucker, Germany), using Cu Kα radiation over the range of 20–70°. The average crystallite size of the samples was calculated from the diffraction peak broadening as described by Kondo et al.[30]

Transmission Electron Microscope (TEM)

The morphology (particle size and shape) of the undoped and N-doped TiO_2 NPs were observed by a transmission electron microscope (TEM) (JEM1010, JEOL, Japan), operating at 80 kV.

X-ray Photoelectron Spectroscopy (XPS)

The chemical states of N in the N-TiO_2 NPs were analyzed using x-ray photoelectron spectroscopy (Model S-Probe™2803, Fisons Instruments, USA). The XP spectra were acquired using monochromatic Al-K radiation (100 W), and the core levels of N_{1s} were calibrated with respect to the C_{1s} level at 284.5 eV.

Bunauer–Emmett–Teller (BET)

The Bunauer-Emmett-Teller specific surface area (S_{BET}) of the prepared samples was measured by N_2 adsorption/desorption isotherm at 77 °K using an ASAP 2010 Micromeritics adsorption apparatus (USA).

Measurement of Photocatalytic Activity

The photocatalytic reaction of as-synthesized N-TiO_2 was conducted using light source from a 40 W Goldstar compact lamp (Fig. S1). A filter (400-700 nm cut-off wavelengths) was used to block the UV light and let only visible light pass through (Fig. S2). Typically, 150 mg of N-TiO_2 was added into 200 ml aqueous solution of MB (10 mg/L) and stirred in the dark. The dye was allowed to adsorb onto N-TiO_2 before being exposed to the light source. After 90 min of irradiation, the photocatalytic effects were measured by UV spectrophotometer (CECIL—CE 1011, Germany) at 663 nm.[31] The photocatalytic activity of undoped TiO_2 was also measured and used as reference sample. The photocatalytic degradation efficiency of TiO_2 was determined using method of Gouma and Mills.[32]

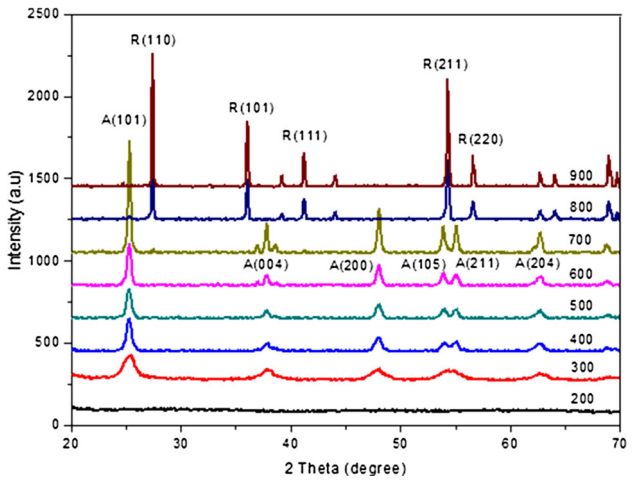

Fig. 1. X-ray diffraction patterns of N-doped TiO_2 at different calcination temperatures (200–900°C). Calcination time is 30 min.

RESULTS AND DISCUSSION

Influence of Calcination Temperature and $NH_3/TiCl_4$ Molar Ratio on Crystallite Structure of N-TiO_2

The mechanism of transformation of titanium precursor into N-TiO_2 was given as below:

$$TiCl_4 + H_2O \rightarrow Ti(OH)_x + Cl^- \quad (1)$$

$$NH_3 + H_2O \rightarrow NH_4OH \quad (2)$$

$$Ti(OH)_x + NH_4OH \rightarrow N - - - Ti(OH)_x + H_2O \quad (3)$$

$$N - - - Ti(OH)_x \rightarrow N - - - TiO_2 + H_2O \quad (4)$$

Clearly, it is very important to control experimental conditions such as calcination temperature and molar ratio in order to improve the crystal quality as well as increase the photocatalytic activity of N-TiO_2 crystals.

Influence of Calcination Temperature on Crystallite Structure of N-TiO_2

The phase transformation of N-TiO_2 from amorphous (<200°C) to anatase (200–600°C) and then rutile (>600°C) is demonstrated in Fig. 1. Obviously, no crystal phase was formed at low calcination temperature of 200°C and the samples were amorphous. At 300°C, the crystals started to grow in anatase phase (ref JCPDS file No. 21–1272). The crystallite structure of the nanoparticles (as

Table I. Influence of calcination temperature on lattice parameters, actual nitrogen content in sample and photocatalytic activity of N-TiO_2

Temperature (°C)	Lattice parameters		Nitrogen content* (%)	Phase composition		Photocatalytic activity (%)
	a = b, Å	c, Å		*A* (%)	*R* (%)	
200	–	–	–	Amorphous	Amorphous	62.5 ± 1.8
300	3.790	9.487	4.51	100	0	70.5 ± 2.0
350	3.789	9.488	4.02	100	0	73.0 ± 2.0
400	3.788	9.500	3.40	100	0	82.5 ± 2.7
500	3.791	9.508	2.43	100	0	94.0 ± 3.5
600	3.787	9.512	1.74	100	0	99.4 ± 3.9
700	3.782	9.512	0.86	91.3	8.7	98.5 ± 3.8
800	–	–	0	0	100	93.0 ± 3.0
900	–	–	0	0	100	83.5 ± 2.8

*N elemental content calculated from XPS spectra.

indicated by the sharpness of the XRD peaks) was improved at higher calcination temperature (400–600°C) due to thermally induced effects on crystal growth. A clear phase transformation from anatase into rutile phase was observed at 700°C. At 800°C and 900°C, only rutile phase (ref JCPDS file No. 21–1276) was noted. In fact, the thermal transformation between rutile phase and anatase phase of N-TiO_2 was reported by many authors and various mechanisms were proposed.[32–34] According to Gouma and Mills,[32] anatase-into-rutile phase transformation was initiated by the formation of rutile nuclei on the surface of anatase particles and the growth of rutile phase was at the expense of neighboring anatase. Zhang and Banfield[33] suggested that rutile nucleation might occur at the interface, surface or in the bulk of TiO_2. Other authors illustrated the absorption of anatase particles onto rutile and the growth of rutile particles by coalescence.[34]

As seen from Table I, with increasing temperature, lattice parameters a and b slightly decreased (3.789 Ῡ 3.782 Å), whereas c increased (9.488 Ῡ 9.512 Å) and reached a stable value of 9.512 Å at 600°C. These results confirmed the improvement in crystal quality of N-TiO_2 samples.

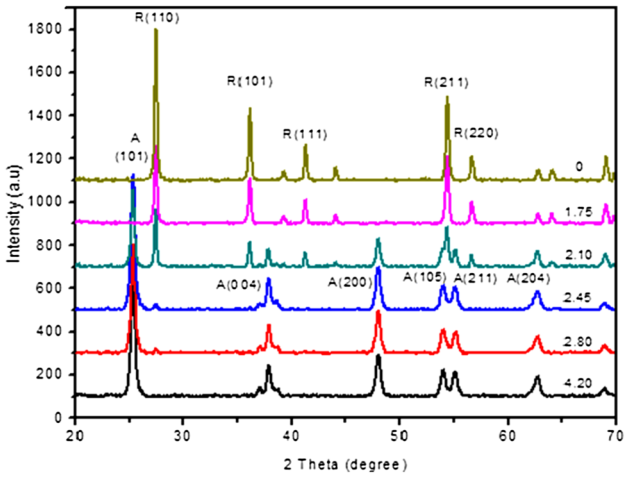

Fig. 2. X-ray diffraction patterns of N-TiO_2 nanoparticles calcined at 600°C at different $NH_3/TiCl_4$ molar ratios.

Influence of Molar Ratio on Crystallite Structure of N-TiO_2

As seen in Fig. 2, N-doping had a remarkable effect on phase transition of TiO_2. At low doping level of nitrogen ($R_N < 2.1$), anatase crystals were completely transformed into rutile after having been annealed at 600°C for 30 min. However, at higher nitrogen content ($R_N = 2.1–4.2$), a mixture of the two phases was observed. At molar ratio as high as 4.2, only pure anatase crystals were obtained and the phase transition occurred only at annealling temperature above 700°C (see "Influence of calcination temperature on crystallite structure of N-TiO2" section). The delay of phase transition could be ascribed to the small size and high porosity of synthesized nanoparticles when doped with nitrogen.[35] Indeed, the phase transformation delay was apparently accompanied by a decrease in particle size (Table II). In previous works, depending synthesis conditions, increase in $NH_3/TiCl_4$ molar ratios might have different effects on crystal sizes. Some works reported that the increase in N content enhanced crystal growth indicated by the increase of crystal sizes.[10] However, in other works, the trend was opposite.[32,36] Under the given conditions of this study, data suggested that doping of nitrogen restrained the growth in particle size of N-TiO_2. The increase in nitrogen content reduced sizes of TiO_2 nanoparticles and inhibited the anatase-to-rutile phase transformation.

These findings showed that phase composition as well as crystal size of N-TiO_2 could be controlled by varying the ratios of ammonia to $TiCl_4$. It was also worth noting that at high level of N-doping ($R_N = 4.2$), pure anatase crystals were obtained with reduced particle sizes. This demonstrated that the agglomeration of TiO_2 nanoparticles might be avoided by N-doping.

Table II. Influence of molar ratio on lattice parameters, actual nitrogen content in sample and photocatalytic activity of N-TiO_2

Molar ratio	Particle size (nm)**	Phase composition		Photocatalytic activity (%)
		A (%)	*R* (%)	
0	32.1 ± 2.2	0	100	42.5 ± 1.4
1.75	30.1 ± 2.1	0	100	60.4 ± 1.8
2.10	25.2 ± 1.5	65.1	34.9	68.6 ± 2.0
2.45	21.2 ± 1.0	93.4	6.6	76.8 ± 2.5
2.80	17.6 ± 0.9	94.2	5.8	85.1 ± 2.9
4.20	17.2 ± 0.9	100	0	99.4 ± 3.9

**Particle size determined from TEM images.

XPS

Figure 3 shows XPS spectra of N-TiO_2 sample prepared at R_N = 4.2 and T_C = 600°C. As seen from Fig. 3, characteristic peaks of Ti 2*p* (459.4 eV) and O 1*s* (529.6 eV) were obtained. The presence of a small peak around 400 eV indicated that nitrogen has been incorporated into TiO_2 lattice. The small peak relevant to nitrogen atoms was actually consisted of three different peaks located at 398, 401.3, and 400 eV (Fig. 4a). The interpretation of binding energies of N 1*s* obtained from XPS spectra was still controversial. In general, peaks at 396–397 eV were usually assigned to *substitutional* nitrogen whereas peaks at higher binding energies were attributed to *interstitial* N.[37,38] In this study, obtained results indicated that the doped nitrogen atoms were apparently interstitial. Specifically, nitrogen has penetrated into lattice and formed Ti–N and O–N bonding rather than replaced oxygen atoms. On the other hand, the XPS spectra also revealed a shift of Ti $2p_{3/2}$ peak from 459.8 eV to 458.5 eV (Fig. 4b) when N was incorporated in the TiO_2. Similarly, characteristic peak of O 1*s* also moved from 531.1 to 530.0 eV (Fig. 4c). These results further confirmed the successful inclusion of N into the TiO_2 crystal.

The XPS peaks relevant to Ti, O, N elements in N-TiO_2 samples prepared at different temperatures were shown in Table III. XPS relevant to Ti and O first shifted toward higher energy levels at the initial stages of growth process of N-TiO_2 crystals, then gradually decreased during the crytallization, as well as phase transformation, and finally reached to intrinsic values of pure samples. On the other hand, XPS spectra provided additional information to reveal how thermal treatment affects structural behaviors of N-TiO_2 nanomaterials.

Meanwhile, a continuous decrease in N 1*s* intensity was observed as increasing calcination temperature. As consequence, the doping level of nitrogen (determined from relative intensities of XPS peaks) in doped samples was found to decline rapidly with increasing temperature from 4.51% to 0%, most probably as a result of nitrogen decomposition from the solid phase. The data obtained from FT-IR spectra (Fig. S3, Supplementary Information) were in agreement with analysis of nitrogen content by XPS (Table I) which showed a continued depletion of nitrogen in N-doped samples as temperatures increased.

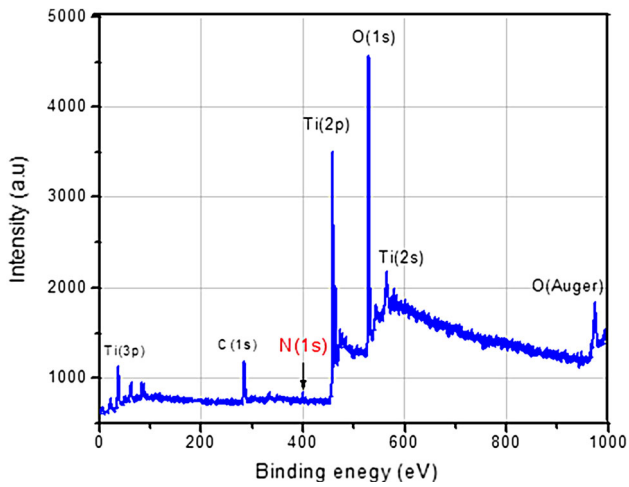

Fig. 3. XPS spectrum of N-TiO_2 nanoparticles annealed at 600°C for 30 min.

Thermal Analysis

Thermal behavior and thermal phase transition of TiO_2 and N-TiO_2 were investigated using Differential thermal analysis (DTA) and Gravimetric thermal analysis (GTA) (Fig. 5). The total weight loss was determined to be 16.60% and 27.48% for undoped and doped TiO_2 nanoparticles, respectively. The mass loss of the doped sample was nearly twice as much as that of pure sample, probably due to desorption of ammonia included in doped samples.[25]

According to Lin et al.[27] the weight loss of these samples can be attributed to (1) evaporation of

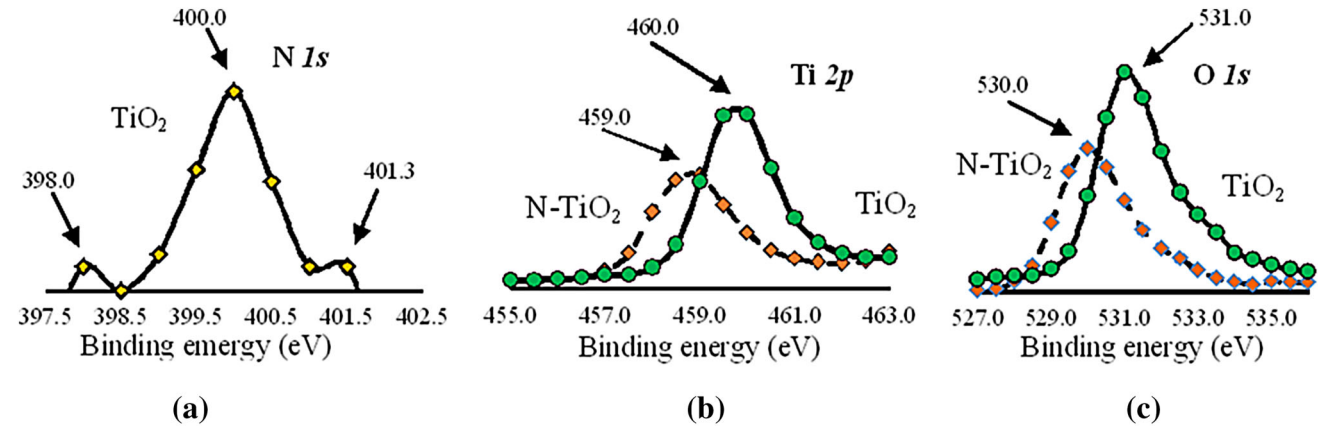

Fig. 4. XPS spectrum of (a) N 1*s*; (b) Ti 2*p*; and (c) O 1*s* of TiO_2 (solid line) nd N-TiO_2 (dash line) calcined at 600°C for 30 min.

adsorbed water and desorption of organic molecules (100–300°C), (2) thermal decomposition of unhydrolyzed precursor (300–450°C), and (3) removal of chemisorbed water (>450°C). As seen from Fig. 5, DTA measurements showed the desorption of adsorbed water including a sharp endothermic peak at low temperatures (122.14°C for pure sample, 129.31°C for doped sample). The removal of water molecules in the mentioned temperature ranges indicated a transformation of titanium precursor into TiO_2 (Eq. 4). Furthermore, an exothermal peak was obtained at 413.2°C in doped sample, which was assigned to the transformation of amorphous TiO_2 into anatase phase.[36,37] Sato et al. [29] also noted exothermic peak at 430°C and ascribed the observed peak to the release of water from oxidation of ammonium at high temperatures. The XPS results (see "XPS" section) evidenced the presence of N–O bonds in N-doped samples. Thus, exothermic peak at 413.2°C probably related to ammonium reaction with oxygen within the molecular lattice.

TEM

Figure 6 illustrated surface morphologies of TiO_2 and N-doped TiO_2 NPs (R_N = 4.2) calcined at 600°C for 30 min. In both cases, the particles that formed the aggregates were nanometric. However, N-TiO_2 particles had smaller size (15–20 nm) than those of undoped material (25–35 nm). This indicated that the presence of nitrogen atoms in TiO_2 lattice units led to reduction in size of nanoparticles.

The effects of N doping on particle sizes of TiO_2 varied with precursors, N sources, synthesis methods and conditions.[29,35] When tetrabutyl titanate was used as the precursor and the synthesis was conducted via hydrothermal process, N-doped, and undoped TiO_2 did not show significant difference in particle size.[35] Similarly, microemulsion-hydrothermal method with the tetrabutyl titanate as the precursor produced N-doped and undoped TiO_2 with very close particle sizes.[8] However, Sathish et al.[28] using $TiCl_3$ and NH_3 to prepare TiO_2 via chemical method, reported significant differences in particle size between pure TiO_2 and N-doped samples. It

Table III. Peak parameters on XPS spectra of the samples prepared at different temperatures

Calcination temperature	O (1*s*)		Ti (2*p*)3/2		Ti (2*p*)1/2		N (1*s*)
	BE, eV	*Δ_{BE}	BE, eV	*Δ_{BE}	BE, eV	*Δ_{BE}	BE, eV
400	531,5	+0,4	460,1	+0,3	466,0	+0,4	397,0; 400,0; 401,0; 402,0; 403,0
500	529,5	−1,6	458,3	−1,5	464,0	−1,6	398,3; 399,1; 400,5; 401,5;
600	530,0	−1,1	458,5	−1,3	464,3	−1,3	$398,0^+$; 400,0; $401,3^+$;
700	530,5	−0,6	459,5	−0,3	464,5	−0,1	$399,0^+$; 405,0; $402,0^+$;
800	531,0	−0,1	459,8	0	465,6	0	No N_{1s} peak

*BE Difference between undoped and doped TiO_2 nanoparticles. BE_{O1s} (TiO_2) = 531,1 eV. $BE_{Ti2p-3/2}$ (TiO_2) = 459,8 eV. $BE_{Ti2p-1/2}$ (TiO_2) = 465,6 eV. $^+$Very weak.

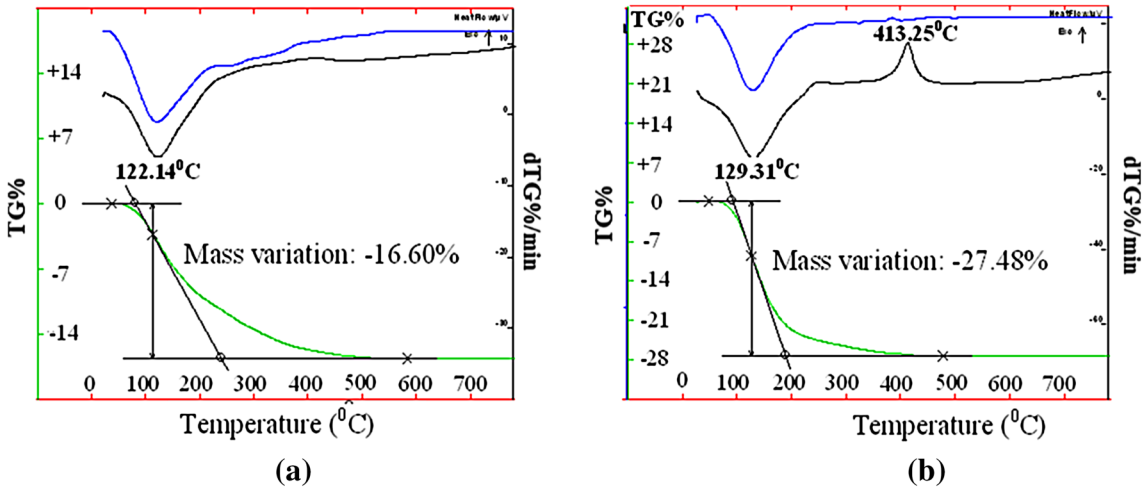

Fig. 5. Thermal analysis of (a) TiO_2 and (b) N-TiO_2 ($NH_3/TiCl_4$ = 4.2) using DTA and GTA. Unannealed samples were dried at 80°C for 24 h before testing.

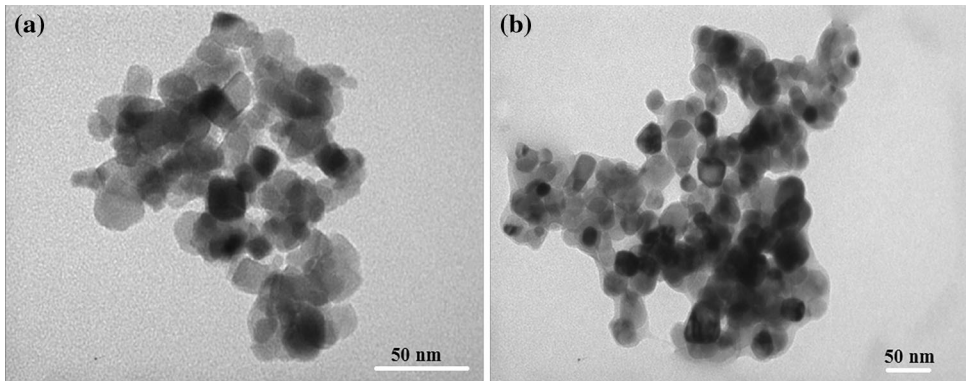

Fig. 6. TEM images of (a) N-TiO_2 and (b) undoped TiO_2 nanoparticles calcined at 600°C for 30 min.

was also important to note that the extent of particle size variations also depended on the amount of N used for doping TiO_2 catalyst.[10]

UV–Vis

The UV–Vis spectra of N-TiO_2 samples were measured to determine the bandgap shift (data not shown here, see Fig. S7).

For all the samples, there was a sharp edge, which could be assigned to the intrinsic bandgap of TiO_2. The presence of nitrogen atoms within TiO_2 lattice was indicated by a noticeable shift of absorption edge to the visible light region as compared to the pure sample (3.2 eV) and a small absorption band at long wavelengths (400–550 nm). It was believed that the inclusion of nitrogen atoms in TiO_2 generated isolated N_{2p} band above the top of the O_{2p} valance band, thereby, narrowed the bandgap energy of the material.[2,29,33]

The calcination temperature is one of the most critical factors affecting optical behaviors of N-TiO_2 samples.[26,29] In this study, the blue shift of absorption edge increased with calcination temperatures up to 600°C. Then, the trend reversed at higher temperatures (Fig. S7). The observed slight expansion of bandgap could be due to the loss of nitrogen at high temperatures. The narrowest bandgap was found to be 2.71 eV. It was worth noting that the color of N-TiO_2 samples varied with the calcination temperatures. The N-TiO_2 samples prepared at R_N of 4.2 and calcined at 200°C, 400°C, 600°C, and 800°C had vivid yellow, yellow, light yellow, and white color, respectively. This color change could be attributed to decreasing amount of nitrogen.

BET

In general, N-doped TiO_2 featured larger surface area than non-doped samples, inferred from smaller crystallite sizes of N-doped TiO_2. Experimentally, the BET surface area of N-TiO_2 (R_N 4.2, 600°C, 30 min) and TiO_2 was estimated to be 66 m^2/g and 12 m^2/g, respectively. The presence of NH_3 molecules could probably lead to better control of nucleation and growth of nanocrystallites, as well as the formation of well-ordered nanostructures. Moreover, the large specific area is critical to enhance activity of photocatalysts.

Photocatalytic Analysis

TiO_2-based catalysts have drawn considerable attention in water treatment and other environmental applications. Therefore, in this study, photocatalytic activity of the as-prepared TiO_2 was evaluated, using methylene blue as a model contaminant. The photocatalytic activities of N-TiO_2 were investigated at different calcination temperatures (Table I) and $NH_3/TiCl_4$ molar ratios (Table II). As the annealing temperature increased, the catalytic power of TiO_2 increased up to 600°C (99.4%) and slightly decreased as the temperature exceeded this limit. The decrease in photocatalytic activity of N-TiO_2 ($T > 600$°C) was reportedly ascribed to removal of nitrogen from TiO_2 matrix at elevated temperature[29] or decreased number of defect sites due to sintering of the samples.[26]

On the other hand, the results clearly showed that photocatalytic decomposition of MB depended on $NH_3/TiCl_4$ ratio. Under studied conditions, catalytic efficiency of Ni-TiO_2 was improved with increasing $NH_3/TiCl_4$ molar ratio and reached a maximum value of 99.4% (R_N = 4.2) (Table II). These results concurred well with those obtained when N-doped TiO_2 was prepared by plasma-assisted chemical vapor deposition[38] and by the sol–gel method using titanium isopropoxide (TTIP) and aqueous ammonia.[27] The trends possibly resulted from the increase in crystallinity and surface area of N-TiO_2 nanoparticles with increasing N/Ti ratio.[27] In this study, the crystal size decreased (up to R_N = 4.2) with increasing amount of N doping (Table II). However, our preliminary experiments (data not shown) demonstrated that as $NH_3/TiCl_4$ molar ratio exceeded 4.2, a decrease in photocatalytic ability of N-TiO_2 was noted. In previous works, this phenomenon was linked to the reduction of surface area.[27] In another research, Huang et al.[35] investigated the effects of urea/$Ti(OH)_4$ ratio on crystal structures and the

photocatalytic activity of the N-TiO_2. Photocatalytic activity was apparently reduced with increasing urea/$Ti(OH)_4$ ratio and the percentage of anatase/rutile phase in the mixture was considered as the major factor. Cong et al. conducted a comprehensive research correlating variations in N/Ti molar ratios to changes in photocatalytic activity of N-TiO_2.[8] Similar trends were observed for N from different sources (thiethylamine, urea, thiourea, hydrazine hydrate). Maximum photocatalytic activity was recorded at an optimal N/Ti ratio and, beyond this value, the photocatalysis of N-TiO_2 decreased significantly. Analysis of actual N content in the sample revealed that optimal Ti/N ratio corresponded to the maximum amount of actual N in the sample. Other explanations included the synergic effect of the pure anatase phase structure, crystallite size, specific surface area, pore volume, and crystallinity of the sample.[10]

CONCLUSION

In summary, a simple approach for the synthesis of nitrogen-doped TiO_2 nanoparticles has been developed via sol–gel method using $TiCl_4$ and NH_3. The effects of critical factors on structure and photocatalytic properties of the products were evaluated. The results reveal the evolution of TiO_2 crystallite during calcination at different temperatures which will help to select the optimal condition for TiO_2 production. The effects of NH_3 amount on product were also investigated. The data allow the control of the synthesis regarding the process parameters and final product properties. The interstitial nitrogen atoms within TiO_2 lattice units played an important role to generate intermediate energy levels and to narrow the bandgap, thereby enhances VLA of the materials. The advances of the developed strategy could be listed as: (1) easy manipulation; (2) high purity of the obtained products; (3) the controllable level of nitrogen doping; (4) highly photoactive product (up to 1.1% per min for MB); and (5) high anatase-to-rutile phase transformation temperature.

ACKNOWLEDGEMENT

Author Loc T. Nguyen was funded by Asian Institute of Technology (AIT) Research Initiation Grant (SERD-2014-1FB).

ELECTRONIC SUPPLEMENTARY MATERIAL

The online version of this article (doi:10.1007/s11664-016-4894-6) contains supplementary material, which is available to authorized users.

REFERENCES

1. F. Fresno, R. Portela, S. Suarez, and J.M. Coronado, *J. Mater. Chem. A* 2, 2884 (2014).
2. M. Pelaez, N.T. Nolan, S.C. Pillai, M.K. Seery, P. Falaras, A.G. Kontos, P.S.M. Dunlop, J.W.J. Hamilton, J.A. Byrne, K. O'Shea, M.H. Entezari, and D.D. Dionysiou, *Appl. Catal. B* 125, 349 (2012).
3. X. Chen and A. Selloni, *Chem. Rev.* 114, 9282 (2014).
4. R. Asahi, T. Morikawa, H. Irie, and T. Ohwaki, *Chem. Rev.* 114, 9852 (2014).
5. M.M. Khan, S.A. Ansari, D. Pradhan, M.O. Ansari, D.H. Han, J. Lee, and M.H. Cho, *J. Mater. Chem. A* 2, 644 (2014).
6. C. Andriamiadamanana, C. Laberty-Robert, M.T. Sougrati, S. Casale, C. Davoisne, S. Patra, and F. Sauvage, *Inorg. Chem.* 53, 10139 (2014).
7. Z.K. Zheng, B.B. Huang, X.Y. Qin, X.Y. Zhang, Y. Dai, and M.H. Whangbo, *J. Mater. Chem.* 21, 9087 (2011).
8. M.V. Dozzi, L. Artiglia, G. Granozzi, B. Ohtani, and E. Selli, *J. Phys. Chem. C* 118, 25589 (2014).
9. R. Asahi, T. Morikawa, T. Ohwaki, K. Aoki, and Y. Taga, *Science* 293, 271 (2001).
10. G. Yang, Z. Jiang, H. Shi, T. Xiao, and Z. Yan, *J. Mater. Chem.* 20, 5309 (2010).
11. J. Xu, P. Sun, X. Zhang, P. Jiang, W. Cao, P. Chen, and H. Jin, *Mater. Manuf. Process.* 29, 1167 (2014).
12. A.V. Emeline, V.N. Kuznetsov, V.K. Rybchuk, and N. Serpone, *Int. J. Photoenergy*, Article ID 258394, 19 (2008).
13. M. Batzill, E.H. Morales, and U. Diebold, *Phys. Rev. Lett.* 96, 026103 (2006).
14. X.B. Chen, Y.B. Lou, A.C.S. Samia, C. Burda, and J.L. Gole, *Adv. Funct. Mater.* 15, 49 (2005).
15. A.V. Emeline, N.V. Sheremetyeva, N.V. Khomchenko, V.K. Ryabchuk, and N. Serpone, *J. Phys. Chem. C* 111, 11462 (2007).
16. C. Wang, Q. Hu, J. Huang, L. Wu, Z. Deng, Z. Liu, Y. Liu, and Y. Cao, *Appl. Surf. Sci.* 283, 192 (2013).
17. C. Guillén, J. Montero, and J. Herrero, *J. Alloys Compd.* 647, 506 (2015).
18. A. Borras, C. Lopez, V. Rico, F. Gracia, A.R. Gonzalez-Elipe, E. Richter, G. Battiston, R. Gerbasi, N. McSporran, G. Sauthier, E. Gyorgy, and A. Figueras, *J. Phys. Chem. C* 111, 1808 (2007).
19. C.W. Dunnill and I.P. Parkin, *Dalton Trans.* 40, 1640 (2011).
20. Y. Guo, X.W. Zhang, W.H. Weng, and G.R. Han, *Thin Solid Films* 515, 7121 (2007).
21. M.J. Powell, C.W. Dunnill, and I.P. Parkin, *J. Photochem. Photobiol. A* 281, 34 (2014).
22. S. Livraghi, M.C. Paganini, E. Giamello, A. Selloni, C. Valentin, and G. Pacchioni, *J. Am. Ceram. Phys. Chem. B* 108, 17273 (2004).
23. S. Sato, *Chem. Phys. Lett.* 123, 128 (1986).
24. S. Sato, R. Nakamura, and S. Abe, *Appl. Catal. A* 284, 137 (2005).
25. T. Morikawa, R. Asahi, T. Ohwaki, K. Aoki, and Y. Taga, *J. Appl. Phys.* 40, L561 (2001).
26. T. Sano, N. Negishi, K. Koike, K. Takeuchi, and S. Matsuzawa, *J. Mater. Chem.* 14, 380 (2004).
27. Y.T. Lin, C.H. Weng, H.J. Hsu, Y.H. Lin, and C.C. Shiesh, *Int. J. Photoenergy* 2013, 268723 (2013). doi:10.1155/2013/268723.
28. M. Sathish, B. Viswanathan, R.P. Viswanath, and C.S. Gopinath, *Chem. Mater.* 17, 6353 (2005).
29. X.Z. Bu, G.K. Zhang, and C.H. Zhang, *Appl. Surf. Sci.* 258, 8001 (2012).
30. T. Kondo, K. Shindo, M. Arakawa, and Y. Sakurai, *J. Alloys Compd.* 375, 291 (2004).
31. P.I. Gouma and M.J. Mills, *J. Am. Ceram. Soc.* 84, 621 (2001).
32. H. Zhang and J.F. Banfield, *J. Mater. Res.* 15, 448 (2000).
33. G.H. Lee and J.M. Zuo, *J. Am. Ceram. Soc.* 87, 479 (2004).
34. D.H. Chen, F.Z. Huang, L. Cao, Y.B. Cheng, and R.A. Caruso, *Chem. A Eur. J.* 18, 13769 (2012).

35. N.T. Nolan, D.W. Synnott, M.K. Seery, S.J. Hinder, W.A. Van, and S.C. Pillai, *J. Hazard. Mater.* 211–212, 94 (2012).
36. D. Di Valentin, E. Finazzi, G. Pacchioni, A. Selloni, S. Livraghi, M.C. Paganini, and E. Giamiello, *Chem. Phys.* 339, 56 (2007).
37. H. Shen, L. Mi, P. Xu, W.D. Shen, and P.N. Wang, *Appl. Surf. Sci.* 253, 7028 (2007).
38. S. Buzby, M.A. Barakat, H. Lin, C. Ni, S.A. Rykov, J.G. Chen, and S.I. Shah, *J. Vac. Sci. Technol. B* 24, 1214 (2006).